Editors' Suggestion

# Electron-phonon coupling in graphene placed between magnetic Li and Si layers on cobalt

Dmitry Yu. Usachov,[1,*] Alexander V. Fedorov,[1,2] Oleg Yu. Vilkov,[1] Ilya I. Ogorodnikov,[3] Mikhail V. Kuznetsov,[3] Alexander Grüneis,[4] Clemens Laubschat,[5] and Denis V. Vyalikh[1,6,7]

[1]*St. Petersburg State University, Physical Department, 7/9 Universitetskaya Naberezhnaya, St. Petersburg 199034, Russia*

[2]*IFW Dresden, P.O. Box 270116, 01171 Dresden, Germany*

[3]*Institute of Solid State Chemistry, Ural Branch of the Russian Academy of Sciences, Pervomayskaya Strasse 91, 620990 Ekaterinburg, Russia*

[4]*II Institute of Physics, University of Cologne, Zülpicher Strasse 77, 50937 Cologne, Germany*

[5]*Institute of Solid State and Materials Physics, Technische Universität Dresden, 01062 Dresden, Germany*

[6]*Departamento de Fisica de Materiales and CFM-MPC UPV/EHU, Donostia International Physics Center, 20080 San Sebastian, Spain*

[7]*IKERBASQUE, Basque Foundation for Science, 48011 Bilbao, Spain*

(Received 2 December 2017; published 21 February 2018)

Using angle-resolved photoemission spectroscopy (ARPES), we study the electronic structure and electron-phonon coupling in a Li-doped graphene monolayer decoupled from the Co(0001) substrate by intercalation of silicon. Based on the photoelectron diffraction measurements, we disclose the structural properties of the Si/Co interface. Our density functional theory calculations demonstrate that in the studied Li/graphene/Si/Co system the magnetism of Co substrate induces notable magnetic moments on Li and Si atoms. At the same time graphene remains almost nonmagnetic and clamped between two magnetically active atomic layers with antiparallel magnetizations. ARPES maps of the graphene Fermi surface reveal strong electron doping, which may lead to superconductivity mediated by electron-phonon coupling (EPC). Analysis of the spectral function of photoelectrons reveals apparent anisotropy of EPC in the $k$ space. These properties make the studied system tempting for studying the relation between superconductivity and magnetism in two-dimensional materials.

DOI: 10.1103/PhysRevB.97.085132

## I. INTRODUCTION

Many-body interactions in crystalline solids and their peculiarities result in a wealth of extraordinary properties and phenomena like Kondo and heavy-fermions behavior, Mott transition, formation of charge and spin density waves, superconductivity, and many others. In conventional models of superconductivity the formation of Cooper pairs was conclusively established to be the result of strong electron-phonon coupling (EPC). Recently, the breakdown of the high-temperature superconductivity (more than 200 K) was demonstrated for the conventional phonon-driven superconductor $H_2S$ gas at very high pressure [1]. However, the majority of materials exhibit lower transition temperatures. For example, superconductivity in graphite intercalation compounds (GICs), which were intensively studied in the past, reveals a maximum superconducting transition temperature $T_C$ of 11.5 K for Ca-doped graphite with a stoichiometry of $CaC_6$ [2,3]. The appearance of superconductivity in this material was explained by strong EPC, which appears upon Ca doping. Further theoretical calculations [4] demonstrate that there are three major contributions to EPC that arise from (i) in-plane C phonons ($C_{xy}$) coupled to $\pi^*$ electrons, (ii) in-plane Ca phonons ($Ca_{xy}$) coupled to $\pi^*$ electrons, and (iii) out-of-plane C phonons ($C_z$) coupled to the Ca electronic band. Subsequent angle-resolved photoemission spectroscopy (ARPES) measurements with sophisticated analysis of the spectral function confirmed the first and the third contributions [5], while observation of $Ca_{xy}$ phonons currently seems beyond the possibilities of ARPES instruments.

Observation of superconductivity in Ca-doped graphite has renewed and initiated further studies of graphite intercalation compounds in order to deeply understand the EPC and its relation with superconductivity. Recent ARPES studies of graphite doped with Li, K, and Ca have shown that EPC strength and $T_C$ steadily depend on the filling of the $\pi^*$ band [6–8]. From these observations it was concluded that the major role of intercalants is to provide the charge to the graphene bands, while superconductivity mostly originates from the graphene sheets [8]. However, this is in contradiction to the theoretical studies that have established the significant role of the interlayer metal bands [4,9].

The studies of GICs have raised a question about the possibility of superconductivity in single and bilayer graphene doped with alkaline and alkaline-earth metals. For example, it was theoretically predicted that a Li-covered graphene monolayer would become superconducting at 8.1 K (in contrast to the nonsuperconducting bulk $LiC_6$ GIC), while Ca-doped graphene may have a much smaller $T_C$ of about 1.4 K due to strong EPC [9]. It was proposed that the reason for such a difference is the much stronger EPC in the $LiC_6$ system due to the interlayer band which crosses the Fermi level $E_F$. Using ARPES, the superconducting gap in Li-doped graphene formed on SiC was directly measured, and $T_C =$ 5.9 K was estimated [10]. Direct proof of superconductivity in such graphene-based systems came recently from transport measurements which found $T_C = 4$–6 K in Ca-doped graphene

*dmitry.usachov@spbu.ru

 ©2018 American Physical Society

laminates [11] and $T_C = 2$ K for Ca-doped bilayer graphene grown on a SiC substrate [12].

The ARPES studies of GICs have demonstrated that EPC is indeed anisotropic in $k$ space [6,7,13]. Further ARPES measurements of a K-doped single graphene layer on gold [14] and a Rb-intercalated bilayer graphene on SiC [15] have also revealed strong anisotropy of EPC. A rather recent systematic ARPES study of graphene monolayer on Au and Ge doped with different metals has shown that anisotropy is seen for all these cases [16] and for any kind of dopant with maximal predicted $T_C = 1.5$ K for Ca-doped graphene [17]. In the case of a graphene monolayer, the anisotropy is observed for the low-energy part of the $k$-resolved Eliashberg function below 80 meV [17], and the nature of these low-energy phonon modes remains unclear.

Previous studies [16,17] of anisotropic low-energy phonon modes contributing to EPC were limited to the analysis of only two symmetric directions in the Brillouin zone (BZ) of graphene. Here we perform an analysis of both symmetric and nonsymmetric directions in BZ. We explore the crystal and electronic structures of a multilayer graphene/Si/Co(0001) system doped with lithium. We also consider contributions of different phonon modes to EPC and analyze the effect of the substrate material on the doping level and EPC strength in graphene. One of the curious results of our work is that density-functional theory (DFT) analysis suggests that Si- and Li-related bands become strongly spin polarized due to exchange interaction with the ferromagnetic Co substrate. Thus, we can conclude that here graphene lies between two magnetically active layers and at the same time exhibits strong and highly anisotropic EPC experimentally derived from ARPES measurements. This makes this system rather tempting for studying possible superconductivity and its relation to magnetism.

## II. METHODS

Single-layer graphene was synthesized under ultrahigh-vacuum (UHV) conditions by chemical-vapor deposition on crystalline Co(0001) film with a thickness of ~10 nm, deposited on a clean W(110) surface. The base pressure in the UHV chamber was $2\times10^{-10}$ mbar. The low-energy electron diffraction (LEED) patterns of the metal film showed a sharp $(1\times1)$ hexagonal pattern, indicating its good crystallinity. The graphene synthesis was performed as follows: The substrate was heated up to a temperature of 650 °C; then propylene ($C_3H_6$) with a pressure of $10^{-6}$ mbar was introduced into the UHV chamber for 15 min. Under these conditions graphene growth starts immediately on the hot metal surface and stops when the catalytically active metal is passivated with a single graphene layer [18,19]. The synthesis of graphene was performed at the Resource Center "Physical Methods of Surface Investigation" of the Research Park of Saint Petersburg State University (SPbU).

After synthesis, the graphene/Co sample was transferred to the ARPES setup through the atmosphere. As shown recently, in the case of a well-oriented graphene layer considered in the present study exposure to air does not affect the interface between graphene and the Co(0001) substrate [19]. The clean graphene surface was restored by annealing the sample in UHV at a temperature of 500 °C. Further silicon intercalation under graphene was performed by deposition of 5 Å of Si followed by annealing at 600 °C. This procedure was repeated several times until homogeneous decoupling of graphene from Co was reached. This was evidenced by a single C 1$s$ peak in the x-ray photoemission spectroscopy (XPS) spectrum and a Dirac cone in the ARPES spectra in agreement with the published data [20,21].

The XPS and ARPES measurements were carried out using the RGBL-2 SR-ARPES station at the UE-112 PGM-1 beamline of the BESSY II synchrotron radiation facility (Helmholtz-Zentrum Berlin). For ARPES measurements a photon energy of 36 eV was used, and the temperature was about 20 K; the energy resolution was not worse than 10 meV. The XPS spectra were acquired at a photon energy of 350 eV at an angle of ~36° from the surface normal.

The calculations of photoelectron diffraction were performed using multiple-scattering formalism (MSC) implemented in the Electron Diffraction in Atomic Clusters (EDAC) program [22]. The Si-Co distance, the two upper interlayer distances in the cobalt substrate, the inner potential, the surface boundary position, and the Debye temperature were varied to achieve the best agreement with experiment. For quantitative estimation of agreement between calculated and measured diffractograms, an $R$-factor analysis was used as defined in Ref. [23].

The DFT calculations were carried out within the generalized gradient approximation to the exchange-correlation potential in the Perdew-Burke-Ernzerhof version [24] as implemented in the FPLO-14.00-48 code (improved version of the original FPLO code by Koepernik and Eschrig [25]). The system was modeled using an eight-layer-thick Co film with the studied atomic layers (Si, graphene, and Li) on both sides. The atomic positions were relaxed until the forces on each atom were less than $10^{-2}$ eV/Å. A $k$-point grid of $8\times8\times1$ was used to sample the BZ. We have considered fcc and hcp positions of Si atoms and found that the fcc location is more favorable for both Si/Co and graphene/Si/Co systems. The energy difference between the fcc and hcp positions was 33 meV. The equilibrium distance between graphene and Si was found to be nearly 3.3 Å.

Our approach for EPC-related analysis of the ARPES data is based on Refs. [17,26–30] and described in Ref. [31].

## III. RESULTS AND DISCUSSION

### A. Crystal structure

The LEED pattern of the graphene/Co system has demonstrated a perfect hexagon image with sharp spots and a rather low background (see Fig. 1). This indicates that the created single-layer graphene is well oriented and forms a sharp interface with the substrate; thus, their lattices fit very well with each other. This is also evidenced from XPS measurements. Inspecting the C 1$s$ spectrum, we could clearly resolve the splitting of the 1$s$ line into two components, which unambiguously correspond to the two carbon sublattices [18]. According to our previous study [18], the right feature corresponds to the C sublattice located atop Co atoms, while the left peak originates from the C sublattice adsorbed above the hollow sites of the Co substrate. Note that the intensities of these two peaks are not equal due to photoelectron diffraction effects [18].

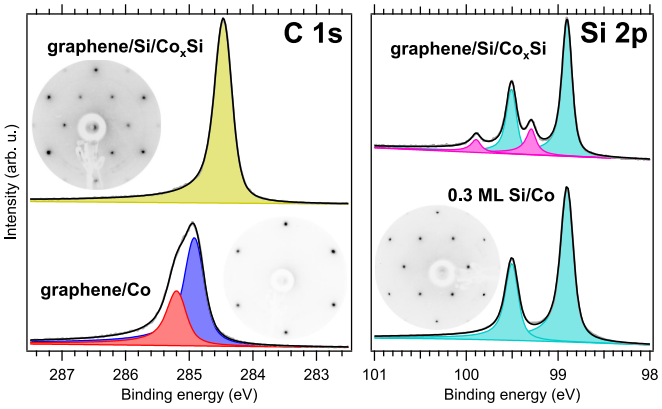


FIG. 1. XPS spectra and corresponding LEED patterns of graphene/Co(0001), graphene/Si/Co$_x$Si, and 0.3 ML of Si atoms adsorbed on the Co(0001) surface.

After deposition and intercalation of silicon at the elevated temperature the XPS spectrum transforms, and C 1$s$ now reveals a single peak which is shifted to lower binding energies. This observation suggests that the interface is changed, and Si atoms penetrating inside modify it, essentially unleashing graphene from strong interaction with the Co surface [20]. At the same time the LEED pattern also undergoes modifications, and now it shows formation of a $(\sqrt{3}\times\sqrt{3})R30^\circ$ structure. To prove that this structure originates from a Co(0001) surface modified by silicon atoms, we have performed a test experiment and deposited about 0.3 monolayer (ML) of Si on a clean Co(0001) film. After annealing at 500 °C the Si/Co system demonstrated a rather similar $(\sqrt{3}\times\sqrt{3})R30^\circ$ structure. The XPS spectrum taken from such system reveals a single spin-orbit doublet with the Si $2p_{3/2}$ component at 98.9 eV of binding energy (BE; see Fig. 1). A similar doublet was also seen after intercalation of Si underneath graphene on Co(0001). However, in the latter case another doublet with significantly lower intensity can be detected at an energy of 99.3 eV. Our analysis suggests that this corresponds to a solid solution of Si in the Co film [21]. Thus, we may conclude that silicon intercalation leads to the formation of a graphene/Si/Co$_x$Si system with $x \geqslant 6$ according to the quantitative XPS analysis [21].

The performed test experiment therefore allows us to conclude that silicon atoms form similar structures on a bare Co surface and underneath graphene. In that regard, the essential question will be the structure of the Si/Co interface. In general, Si atoms may either be adsorbed on the Co surface or form an alloy, as proposed in previous works [20,21]. In order to explore this point and determine the positions of Si atoms, we have measured the dependence of the photoemission intensity of the Si 2$p$ line as a function of the photon energy using the normal emission geometry of the experiment, which is called angle-resolved photoemission extended fine structure. Due to the photoelectron diffraction effect this dependence is a fingerprint of the local atomic structure around the Si atoms. In addition to that to determine the Si/Co(0001) interface structure, we have carried out calculations of photoelectron diffraction.

The respective data obtained for different arrangements of Si atoms at the Co substrate along with the experimental results for the graphene/Si/Co system are shown in Fig. 2. In

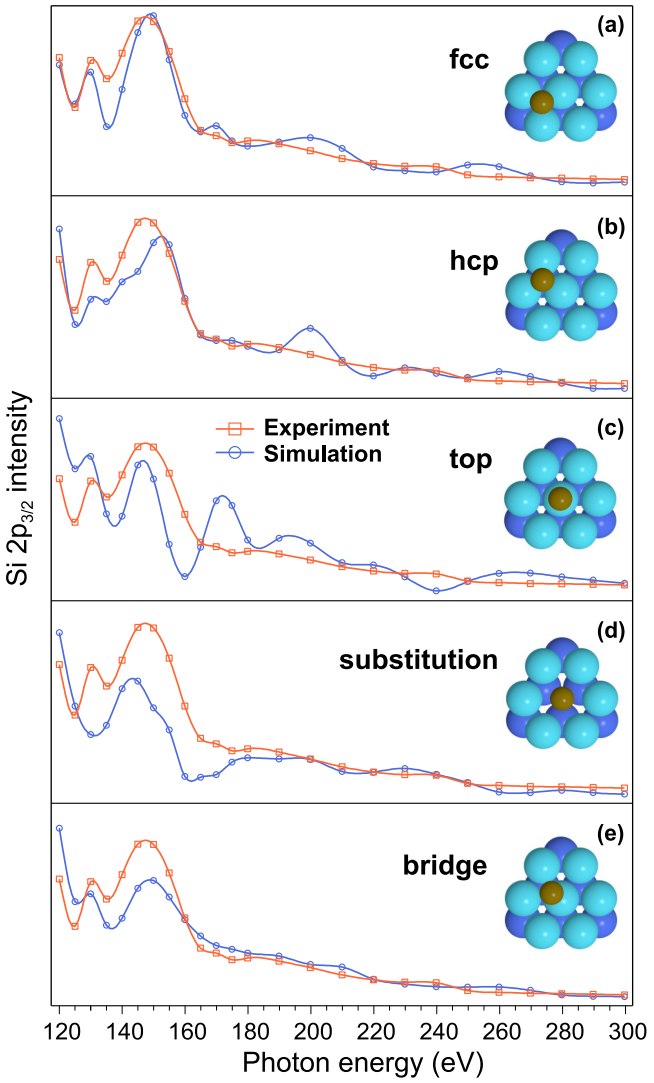


FIG. 2. Calculated and measured intensities of the Si $2p_{3/2}$ XPS peak as a function of photon energy in the normal emission direction for the Si/Co system.

calculations, we have considered the $(\sqrt{3}\times\sqrt{3})R30^\circ$ structure of the adsorbate that was seen in LEED. The best agreement was achieved when Si atoms occupy fcc sites, i.e., when they are located above the octahedral cavities of the Co(0001) substrate. The optimal Si-Co distance was found to be 1.75 Å in both photoelectron diffraction and DFT calculations. The hcp adsorption sites also have reasonable agreement with the experiment; however, our DFT calculations showed that fcc sites are more energetically favorable. Based on these results, we propose the structural model shown in Fig. 3, where Si atoms occupy fcc sites and the C atoms of graphene remain in the top-fcc positions, which is the most favorable structure for the initial graphene/Co system [18].

### B. Electronic structure

The electronic structure of graphene on Co(0001) and in particular its $\pi$ states undergo essential modifications upon Si intercalation. For the native graphene/Co(0001) system the

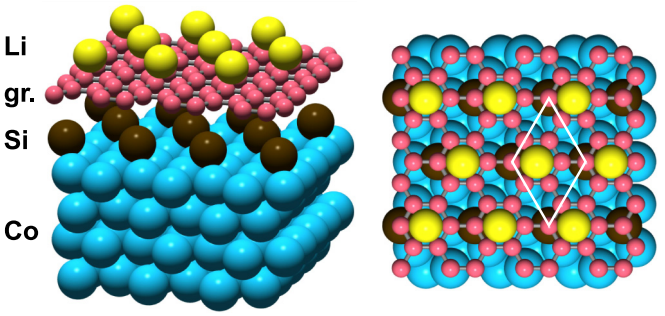


FIG. 3. Structural model of the Li/graphene/Si/Co(0001) system.

Dirac cone band shows splitting in two components due to strong mixing of the C $2p$ and Co $3d$ states [18,32]. After penetration of Si underneath graphene, the Dirac cone is almost restored, and its dispersion becomes similar to that of freestanding graphene. This can be nicely seen in Fig. 4. The interaction with the substrate leads to only a minor $n$-type doping of 0.15 eV. Such a tiny doping effect does not allow us to detect the presence or absence of a band gap in the electron-energy spectrum close to the Fermi energy $E_F$.

The obtained ARPES data are fully consistent with the results of DFT calculations performed for the graphene/Si/Co(0001) system, as shown in Fig. 5. Ferromagnetism of the cobalt substrate leads to spin splitting of not only Co states but Si-derived states as well. For example, the unoccupied surface state which stems from Si atoms is easily seen in the projected band gap around the $K$ point. The magnetic moment of Si atoms was found to be $0.26\mu_B$ and is aligned antiparallel to the magnetic moment of Co atoms. The magnetic moment of C atoms, however, does not exceed $0.008\mu_B$, and therefore, the $\pi$ and $\pi^*$ bands of graphene exhibit negligible spin splitting. Our calculation confirms that graphene of the considered system is quasifreestanding. This is supported by the absence of hybridization between the electronic states of carbon and the

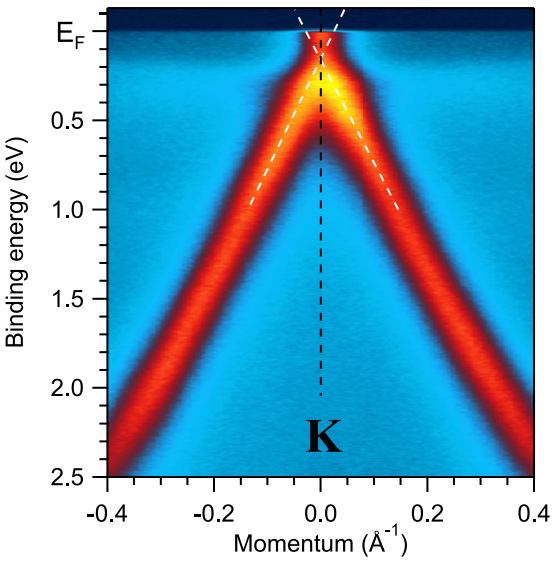


FIG. 4. ARPES spectrum of graphene on the Co(0001) surface after silicon intercalation.

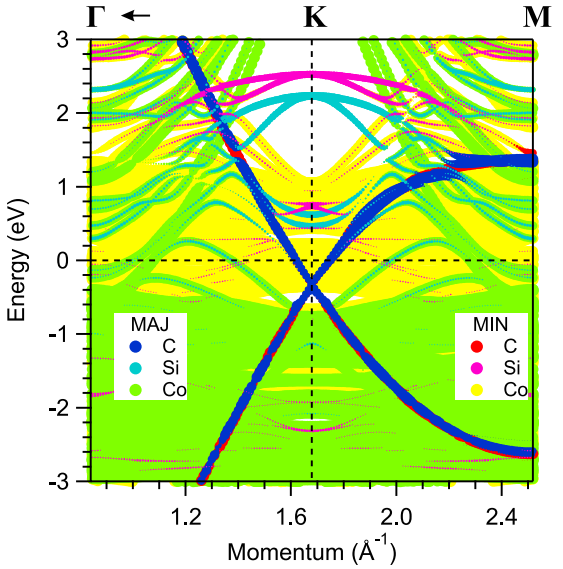


FIG. 5. Calculated electronic structure of the graphene/Si/Co(0001) system. The spot size is proportional to the contribution of selected states to the wave function. The bands of graphene are unfolded and presented along the high-symmetry directions of the BZ of the $(1\times1)$ structure. Labels MAJ and MIN denote majority- and minority-spin directions.

substrate. The latter prevents the strong exchange interaction with the underlying substrate and consequently leads to the absence of magnetism in graphene. However, the underlying Si-Co substrate is magnetic, with a notable moment at Si atoms. A closer look at the $E_F$ region also suggests that the $\pi$ band is almost unperturbed and there is no band gap at the Dirac point. Only a tiny $n$-type charge doping is seen, which is in agreement with the experiment.

After deposition of Li on top of the graphene/Si/Co system the ARPES data demonstrate a strong charge doping of graphene. This is clearly visible in Figs. 6(a) and 6(b), where the Dirac point appears to be shifted to an energy of 1.6 eV below $E_F$. The best description of the $\pi$-band dispersion is achieved when we assume a gap of $\sim$0.4 eV at the $K$ point. The possible nature of the gap is explained in Ref. [33]. Briefly, in the tight-binding description the gap opening is related to changes in the hopping integrals of the C-C bonds around the Li atoms when they are adsorbed in the centers of hexagons and form a $(\sqrt{3}\times\sqrt{3})R30^\circ$ structure, which is commonly observed in Li-intercalated graphite. We cannot prove that in our sample Li atoms form such a structure because the corresponding LEED pattern cannot be distinguished from the LEED pattern of the Si layer, which has the same unit cell. However, the band gap observation allows us to suppose that in our system Li atoms tend to form a $(\sqrt{3}\times\sqrt{3})$ structure on the graphene surface. To prove that Li remains mainly at the graphene surface, we performed angle-dependent XPS measurements (not shown). Their results indicate that at the grazing angle the ratio of the signals from Li $1s$ to C $1s$ is higher than that for the normal emission, implying that Li atoms remain primarily on top of graphene.

Figure 6(c) shows the results of DFT calculation of the electronic bands for the Li/graphene/Si/Co system with the

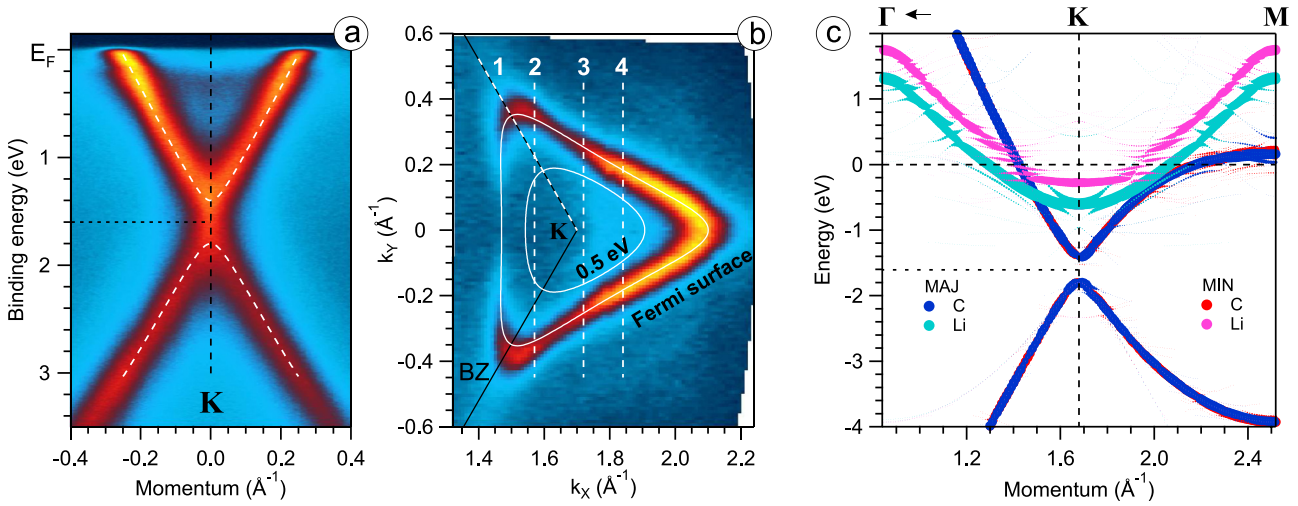


FIG. 6. Electronic structure of the Li/graphene/Si/Co(0001) system: (a) ARPES view of the Dirac cone, (b) ARPES map of the Fermi surface, and (c) DFT calculation. For simplicity, in the DFT results only the contributions of Li and C atoms to the electronic bands are shown. The contribution of carbon states is unfolded for better comparability with the ARPES data.

structure shown in Fig. 3. These results give a Dirac point BE of 1.6 eV and a gap width of 0.4 eV, which are in perfect agreement with the ARPES observations. Such agreement supports the validity of the proposed structural model for the analysis of the electronic band structure. Inspecting the computed band structure, we can conclude that the $\pi$ band has negligible spin splitting, similar to the bare graphene/Si/Co system. Calculations suggest that the magnetic moment of carbon atoms does not exceed $0.005\mu_B$. In contrast, Li atoms exhibit a notable magnetic moment of $0.12\mu_B$ that on its own looks curious and can be explained by exchange coupling with Co. Interestingly, the moments of Li are aligned in a parallel manner with the magnetic moment of Co atoms, while Si moments remain in the antiparallel alignment. The exchange spin splitting of the Li $2s$ band is clearly seen in Fig. 6(c), and its value is 350 meV. The magnetic moment of Si atoms remains almost unchanged ($-0.28\mu_B$) upon Li doping. Thus, we can see that graphene is confined from both sides by magnetically active Li and Si layers, where magnetism stems from exchange interaction with the ferromagnetic Co substrate, and the magnetic moments in Li and Si layers are antiparallel to each other.

In Fig. 6(b) we show the Fermi surface map for the Li/graphene/Si/Co system derived from ARPES measurements. If we assume that the density of $\pi$ states remains unchanged upon Li adsorption, then the $k$-space area within the Fermi contour allows us to estimate the charge transfer from Li to graphene that is 0.15 of the electron charge per $(1\times1)$ graphene unit cell. This value corresponds to the concentration of electrons in the conduction band of nearly $3\times10^{14}$ cm$^{-2}$, which is notably higher than the doping level in the Li/graphene/Au/Ni system studied previously with regard to EPC [17]. In our case, inserting a nonmetallic Si layer between graphene and the metallic substrate enhances significantly the doping level of graphene. Thus, the currently considered Li/graphene/Si/Co system becomes rather curious with regard to the subject of EPC, which may lead to a $T_C$ value of more than 8 K according to theoretical estimations [34].

### C. Electron-phonon coupling

It is well known that ARPES data contain information about many-body interactions in crystalline solids when the itinerant electrons couple with different quasiparticles like phonons. Electron-phonon coupling can be visualized as a series of kinklike features in the ARPES data in the vicinity of $E_F$ and has been widely discussed in the past [35]. For our system, the respective kinks can be very well distinguished in the ARPES data shown in Fig. 7.

In order to extract reliable values of the EPC constant the analysis procedure was preliminarily tested on the simulated APRES data [31]. From this analysis we found that in the case when the ARPES data are measured along the direction which does not go through the **K** point of the BZ, reliable results can be obtained only when the momentum distribution curves (MDCs) are approximated with an asymmetric peak function multiplied by a momentum-resolved photoemission cross section of the graphene $\pi$ band. Thus, to fit the MDC profiles we use the following function:

$$\mathrm{MDC}(k) = \left(1 + \left[\frac{k}{\beta + \alpha k}\right]^2\right)^{-1} |C_A(\mathbf{k}) + C_B(\mathbf{k})|^2, \quad (1)$$

where $\beta$ is the peak half width, $\alpha$ is the peak asymmetry, and $C_A(\mathbf{k})$ and $C_B(\mathbf{k})$ are Bloch wave-function amplitudes on the two carbon sublattices. The latter coefficients were determined from the tight-binding approximation of the measured Dirac cone.

Figure 7 shows the ARPES data measured in four different directions of $k$ space. For each direction the Eliashberg function and the EPC constant $\lambda$ were determined using the procedure described in Ref. [31]. Following previous work [17], the Eliashberg function $\alpha^2F(\omega)$ was approximated with three peaks, namely, $p_1$, $p_2$, and $p_3$. This is already enough to achieve good approximations for the real and imaginary parts of the self-energy $\Sigma$, shown in Fig. 7. Peaks $p_2$ and $p_3$, with energies of about 0.16–0.18 eV, correspond to the LO and TO

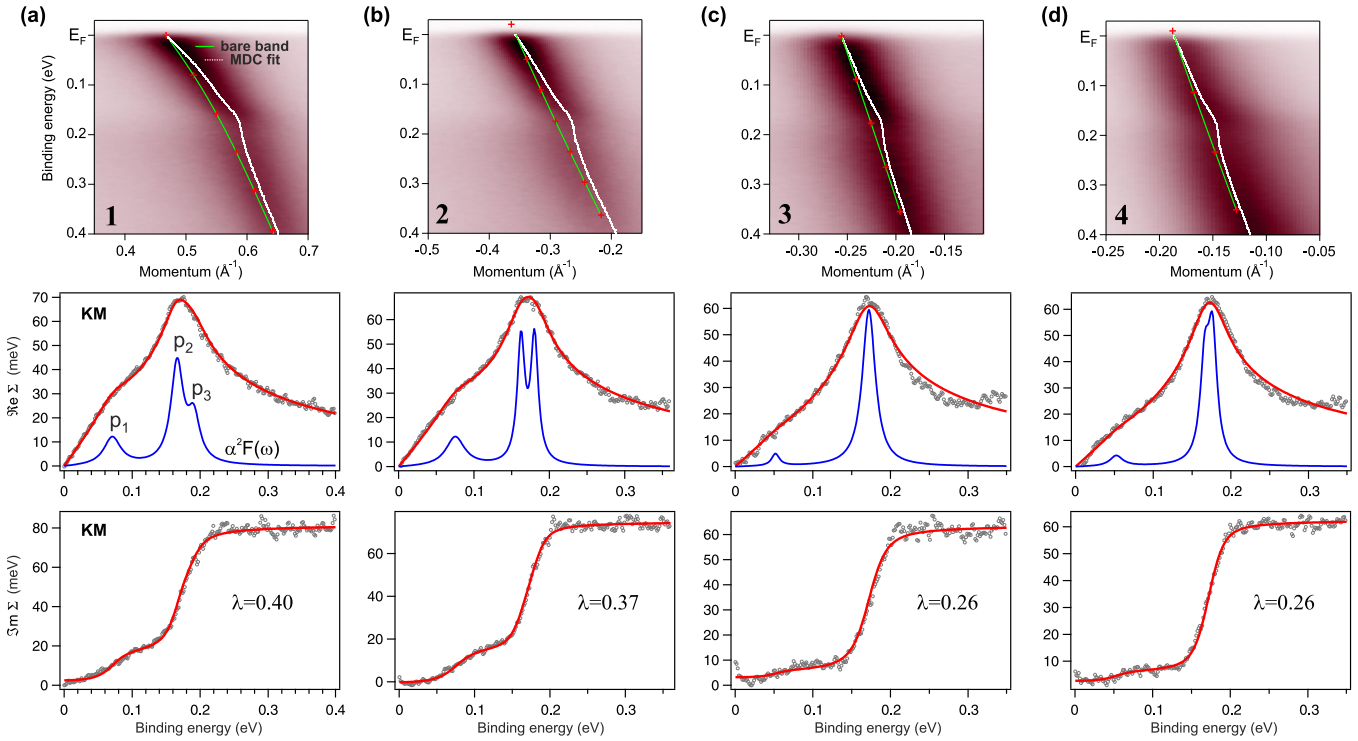


FIG. 7. ARPES data measured along the four directions shown in Fig. 6(b), the corresponding real and imaginary parts of self-energy Σ, and Eliashberg functions $\alpha^2 F(\omega)$ extracted from each of the ARPES maps.

in-plane optical phonons of graphene. They are so close in energy that they can be successfully approximated even with a single peak. Peak $p_1$ has an energy of 50–80 meV. This peak has a maximal intensity in the **KM** direction of the BZ (direction 1 in Fig. 6). For this case the estimated value of the EPC constant reaches $\lambda = 0.40$. The intensity of the $p_1$ mode decreases when the measurement plane moves away from the **KM** direction. This is accompanied by a decrease in λ to a value of 0.26. This kind of anisotropy of EPC was observed for different systems with graphene doped by alkali metals [17]; thus, it is an intrinsic property of doped graphene. However, previous studies were limited to the two high-symmetry directions of BZ. Here we extend the analysis by considering the nonsymmetric directions.

Figure 8 demonstrates how the value of λ is changed in $k$ space when the measurement point is moving along the Fermi contour around the **K** point. It shows that λ reaches a minimum in the **KΓ** direction. The bottom curve in Fig. 8, labeled $\lambda_{23}$, shows the contribution of peaks $p_2$ and $p_3$ to the EPC constant. It can be seen that this contribution exhibits only small variations within the range of 0.21–0.25; thus, it is nearly independent of the direction, in agreement with the theoretical calculation [36]. This observation allows us to conclude that the anisotropy of λ is caused by interaction with low-energy phonons that are related to peak $p_1$.

The nature of the anisotropic peak $p_1$ is not well known. Theory predicts rather isotropic intrinsic EPC in doped graphene [36]. Therefore, this peak should be related to the presence of either the substrate or dopant. Its energy is notably higher than the typical energies of metal-related phonons; thus, it cannot be related to the phonons of the dopant. It should originate either from the out-of-plane phonons or from the in-plane acoustic phonons of graphene. The interaction of the out-of-plane phonons with $\pi$ electrons is negligible in isolated graphene [37]. However, theoretical studies of GICs and doped graphene demonstrate that the presence of metal may lead to strong enhancement of the interaction of out-of-plane graphene phonons with $\pi$ electrons because of coupling to the electronic band of metal [4,9,38]. Nevertheless, self-energy calculations for the Ca-intercalated bilayer graphene demonstrate no apparent anisotropy for the kink at 70 meV [38]. Thus, understanding the nature of the observed anisotropy requires further theoretical studies.

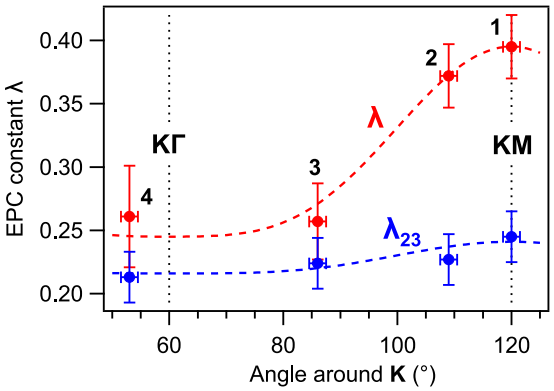


FIG. 8. The top curve shows the measured EPC constant λ as a function of direction. The bottom curve ($\lambda_{23}$) shows the contribution of high-energy phonons ($p_2$ and $p_3$) to the total EPC constant.

## IV. CONCLUSIONS

We have experimentally constructed a system where initially well ordered graphene on a Co(0001) substrate was forced to become quasifreestanding upon Si intercalation. Using photoelectron diffraction, we were able to disclose the structure of the obtained system and explore it theoretically. The first curious result is that the Si layer, which blocks the interplay of graphene with Co, becomes magnetic underneath graphene. Upon further doping with Li atoms, we found that the doping level of graphene becomes essentially higher than, for example, in purely metallic systems such as the widely explored Au-intercalated doped graphene systems. This demonstrates that the substrate plays an essential role in the charge transfer and the value of doping. At the same time, the Li layer above graphene is also magnetic. Like for the Si layer, this is due to exchange magnetism with the Co substrate. Thus, quasifreestanding graphene becomes trapped from both sides by magnetically active Li and Si layers, where the magnetic moments lie in plane and are oriented antiparallel to each other. The latter implies that the C atoms should possess a quite small moment, as we indeed confirmed theoretically.

Analysis of electron-phonon coupling at different points of graphene's Fermi surface demonstrates pronounced anisotropy of the EPC. This anisotropy originates from phonon modes with energies of 50–80 meV, while the contribution from optical phonons at energies of $>160$ meV is almost isotropic. On the one hand, our data imply that in such a graphene-based system superconductivity might be expected at a few kelvin. However, the rather curious exchange magnetism induced in the neighboring Si and Li layers could suppress it. All this makes this system tempting for disentangling the relation between superconductivity and magnetism in ultrathin layers.

## ACKNOWLEDGMENTS

D.Yu.U., D.V.V., and A.V.F. acknowledge SPbU for research Grant No. 11.65.42.2017 and RFBR (Grant No. 17-02-00427). D.Yu.U., I.I.O., and M.V.K. acknowledge RFBR (Grant No. 16-29-06410). C.L. acknowledges DFG (Grant No. LA655-17/1). A.G. and A.V.F. acknowledge ERC Grant No. 648589 "SUPER-2D" and funding from DFG project CRC 1238 (project A1) and DFG project GR 3708/2-1. We acknowledge Helmholtz-Zentrum Berlin für Materialien und Energie for support within the bilateral Russian-German Laboratory program. We cordially thank Prof. E. V. Chulkov for consultations.

[1] A. P. Drozdov, M. I. Eremets, I. A. Troyan, V. Ksenofontov, and S. I. Shylin, Conventional superconductivity at 203 Kelvin at high pressures in the sulfur hydride system, Nature (London) **525**, 73 (2015).

[2] T. E. Weller, M. Ellerby, S. S. Saxena, R. P. Smith, and N. T. Skipper, Superconductivity in the intercalated graphite compounds $C_6$Yb and $C_6$Ca, Nat. Phys. **1**, 39 (2005).

[3] N. Emery, C. Hérold, M. d'Astuto, V. Garcia, Ch. Bellin, J. F. Marêché, P. Lagrange, and G. Loupias, Superconductivity of Bulk $CaC_6$, Phys. Rev. Lett. **95**, 087003 (2005).

[4] M. Calandra and F. Mauri, Theoretical Explanation of Superconductivity in $C_6$Ca, Phys. Rev. Lett. **95**, 237002 (2005).

[5] S.-L. Yang, J. A. Sobota, C. A. Howard, C. J. Pickard, M. Hashimoto, D. H. Lu, S.-K. Mo, P. S. Kirchmann, and Z.-X. Shen, Superconducting graphene sheets in $CaC_6$ enabled by phonon-mediated interband interactions, Nat. Commun. **5**, 3493 (2014).

[6] Z.-H. Pan, J. Camacho, M. H. Upton, A. V. Fedorov, C. A. Howard, M. Ellerby, and T. Valla, Electronic Structure of Superconducting $KC_8$ and Nonsuperconducting $LiC_6$ Graphite Intercalation Compounds: Evidence for a Graphene-Sheet-Driven Superconducting State, Phys. Rev. Lett. **106**, 187002 (2011).

[7] T. Valla, J. Camacho, Z.-H. Pan, A. V. Fedorov, A. C. Walters, C. A. Howard, and M. Ellerby, Anisotropic Electron-Phonon Coupling and Dynamical Nesting on the Graphene Sheets in Superconducting $CaC_6$ Using Angle-Resolved Photoemission Spectroscopy, Phys. Rev. Lett. **102**, 107007 (2009).

[8] T. Valla and Z. Pan, in *Superconductivity and Electron-Phonon Coupling in Graphite Intercalation Compounds, Physics and Applications of Graphene - Experiments*, edited by S. Mikhailov (InTech, Rijeka, Croatia, 2011).

[9] G. Profeta, M. Calandra, and F. Mauri, Phonon-mediated superconductivity in graphene by lithium deposition, Nat. Phys. **8**, 131 (2012).

[10] B. M. Ludbrook, G. Levy, P. Nigge, M. Zonno, M. Schneider, D. J. Dvorak, C. N. Veenstra, S. Zhdanovich, D. Wong, P. Dosanjh, C. Straßer, A. Stöhr, S. Forti, C. R. Ast, U. Starke, and A. Damascelli, Evidence for superconductivity in Li-decorated monolayer graphene, Proc. Natl. Acad. Sci. USA **112**, 11795 (2015).

[11] J. Chapman, Y. Su, C. A. Howard, D. Kundys, A. N. Grigorenko, F. Guinea, A. K. Geim, I. V. Grigorieva, and R. R. Nair, Superconductivity in Ca-doped graphene laminates, Sci. Rep. **6**, 23254 (2016).

[12] S. Ichinokura, K. Sugawara, A. Takayama, T. Takahashi, and S. Hasegawa, Superconducting calcium-intercalated bilayer graphene, ACS Nano **10**, 2761 (2016).

[13] A. Grüneis, C. Attaccalite, A. Rubio, D. V. Vyalikh, S. L. Molodtsov, J. Fink, R. Follath, W. Eberhardt, B. Büchner, and T. Pichler, Electronic structure and electron-phonon coupling of doped graphene layers in $KC_8$, Phys. Rev. B **79**, 205106 (2009).

[14] D. Haberer, L. Petaccia, A. V. Fedorov, C. S. Praveen, S. Fabris, S. Piccinin, O. Vilkov, D. V. Vyalikh, A. Preobrajenski, N. I. Verbitskiy, H. Shiozawa, J. Fink, M. Knupfer, B. Büchner, and A. Grüneis, Anisotropic Eliashberg function and electron-phonon coupling in doped graphene, Phys. Rev. B **88**, 081401 (2013).

[15] J. Kleeman, K. Sugawara, T. Sato, and T. Takahashi, Anisotropic electron-phonon coupling in Rb-intercalated bilayer graphene, J. Phys. Soc. Jpn. **83**, 124715 (2014).

[16] N. I. Verbitskiy, A. V. Fedorov, C. Tresca, G. Profeta, L. Petaccia, B. V. Senkovskiy, D. Yu. Usachov, D. V. Vyalikh, L. V. Yashina, A. A. Eliseev, T. Pichler, and A. Grüneis, Environmental control

of electron–phonon coupling in barium doped graphene, 2D Mater. **3**, 045003 (2016).

[17] A. V. Fedorov, N. I. Verbitskiy, D. Haberer, C. Struzzi, L. Petaccia, D. Usachov, O. Y. Vilkov, D. V. Vyalikh, J. Fink, M. Knupfer, B. Büchner, and A. Grüneis, Observation of a universal donor-dependent vibrational mode in graphene, Nat. Commun. **5**, 3257 (2014).

[18] D. Yu. Usachov, A. V. Fedorov, O. Yu. Vilkov, A. E. Petukhov, A. G. Rybkin, A. Ernst, M. M. Otrokov, E. V. Chulkov, I. I. Ogorodnikov, M. V. Kuznetsov, L. V. Yashina, E. Yu. Kataev, A. V. Erofeevskaya, V. Yu. Voroshnin, V. K. Adamchuk, C. Laubschat, and D. V. Vyalikh, Large-scale sublattice asymmetry in pure and boron-doped graphene, Nano Lett. **16**, 4535 (2016).

[19] D. Yu. Usachov, V. Yu. Davydov, V. S. Levitskii, V. O. Shevelev, D. Marchenko, B. V. Senkovskiy, O. Yu. Vilkov, A. G. Rybkin, L. V. Yashina, E. V. Chulkov, I. Yu. Sklyadneva, R. Heid, K.-P. Bohnen, C. Laubschat, and D. V. Vyalikh, Raman spectroscopy of lattice-matched graphene on strongly interacting metal surfaces, ACS Nano **11**, 6336 (2017).

[20] O. Vilkov, A. Fedorov, D. Usachov, L. V. Yashina, A. V. Generalov, K. Borygina, N. I. Verbitskiy, A. Grüneis, and D. V. Vyalikh, Controlled assembly of graphene-capped nickel, cobalt and iron silicides, Sci. Rep. **3**, 2168 (2013).

[21] D. Yu. Usachov, A. V. Fedorov, O. Yu. Vilkov, A. V. Erofeevskaya, A. S. Vopilov, V. K. Adamchuk, and D. V. Vyalikh, Formation and lithium doping of graphene on the surface of cobalt silicide, Phys. Solid State **57**, 1040 (2015).

[22] F. J. García de Abajo, M. A. Van Hove, and C. S. Fadley, Multiple scattering of electrons in solids and molecules: A cluster-model approach, Phys. Rev. B **63**, 075404 (2001).

[23] R. Dippel, K.-U. Weiss, K.-M. Schindler, P. Gardner, V. Fritzsche, A. M. Bradshaw, M. C. Asensio, X. M. Hu, D. P. Woodruff, and A. R. González-Elipe, A photoelectron diffraction study of the structure of $PF_3$ adsorbed on Ni{111}, Chem. Phys. Lett. **199**, 625 (1992).

[24] J. P. Perdew, K. Burke, and M. Ernzerhof, Generalized Gradient Approximation Made Simple, Phys. Rev. Lett. **77**, 3865 (1996).

[25] K. Koepernik and H. Eschrig, Full-potential nonorthogonal local-orbital minimum-basis band-structure scheme, Phys. Rev. B **59**, 1743 (1999); FPLO, http://www.FPLO.de/.

[26] A. Damascelli, Z. Hussain, and Z.-X. Shen, Angle-resolved photoemission studies of the cuprate superconductors, Rev. Mod. Phys. **75**, 473 (2003).

[27] G. Grimvall, in *The Electron-Phonon Interaction in Metals*, edited by E. Wohlfarth (North-Holland, New York, 1981).

[28] E. W. Plummer, J. R. Shi, S. J. Tang, E. Rotenberg, and S. D. Kevan, Enhanced electron-phonon coupling at metal surfaces, Prog. Surf. Sci. **74**, 251 (2003).

[29] B. Hellsing, A. Eiguren, and E. V. Chulkov, Electron-phonon coupling at metal surfaces, J. Phys.: Condens. Matter **14**, 5959 (2002).

[30] M. Mucha-Kruczyński, O. Tsyplyatyev, A. Grishin, E. McCann, V. I. Fal'ko, A. Bostwick, and E. Rotenberg, Characterization of graphene through anisotropy of constant-energy maps in angle-resolved photoemission, Phys. Rev. B **77**, 195403 (2008).

[31] See Supplemental Material at http://link.aps.org/supplemental/10.1103/PhysRevB.97.085132 for a description of EPC analysis based on the ARPES data.

[32] D. Usachov, A. Fedorov, M. M. Otrokov, A. Chikina, O. Vilkov, A. Petukhov, A. G. Rybkin, Y. M. Koroteev, E. V. Chulkov, V. K. Adamchuk, A. Grüneis, C. Laubschat, and D. V. Vyalikh, Observation of single-spin Dirac fermions at the graphene/ferromagnet interface, Nano Lett. **15**, 2396 (2015).

[33] M. Farjam and H. Rafii-Tabar, Energy gap opening in submonolayer lithium on graphene: Local density functional and tight-binding calculations, Phys. Rev. B **79**, 045417 (2009).

[34] M. Einenkel and K. B. Efetov, Possibility of superconductivity due to electron-phonon interaction in graphene, Phys. Rev. B **84**, 214508 (2011).

[35] J. D. Koralek, J. F. Douglas, N. C. Plumb, Z. Sun, A. V. Fedorov, M. M. Murnane, H. C. Kapteyn, S. T. Cundiff, Y. Aiura, K. Oka, H. Eisaki, and D. S. Dessau, Laser Based Angle-Resolved Photoemission, the Sudden Approximation, and Quasiparticle-Like Spectral Peaks in $Bi_2Sr_2CaCu_2O_{8+\delta}$, Phys. Rev. Lett. **96**, 017005 (2006).

[36] C.-H. Park, F. Giustino, J. L. McChesney, A. Bostwick, T. Ohta, E. Rotenberg, M. L. Cohen, and S. G. Louie, Van Hove singularity and apparent anisotropy in the electron-phonon interaction in graphene, Phys. Rev. B **77**, 113410 (2008).

[37] K. M. Borysenko, J. T. Mullen, E. A. Barry, S. Paul, Y. G. Semenov, J. M. Zavada, M. B. Nardelli, and K. W. Kim, First-principles analysis of electron-phonon interactions in graphene, Phys. Rev. B **81**, 121412 (2010).

[38] E. R. Margine, H. Lambert, and F. Giustino, Electron-phonon interaction and pairing mechanism in superconducting Ca-intercalated bilayer graphene, Sci. Rep. **6**, 21414 (2016).